Integrating incidence-angle compensation in the segmentation of UAVSAR images

Anca Cristea, Anthony P. Doulgeris

University of Tromsø, Norway

anthony.p.doulgeris@uit.no

Abstract

SAR images display a characteristic intensity variation along the range dimension, caused by the fact that the backscattered intensities depend on the incidence angle. In the case of wide-swath images, this intensity variation from near range to far range is significant enough to affect image segmentation performed on absolute intensity values. The effects are an over-segmentation which creates banding in the range direction, as well as the dillution of the real class distinction. In addition, the decay rates vary for different classes, thus reducing the efficiency of previously proposed global-correction methods.

We propose an unsupervised segmentation method that incorporates the incidence-angle variation into the standard mixture modeling. We demonstrate its efficiency on UAVSAR images containing oil spills and ships on an open-water background, acquired in the North Sea during 2015 (the NORSE2015 experiment). By considering the intensities of the HH channel and an incidence angle range spanning from 30 to 60 degrees, the proposed algorithm is able to remove the banding effect and to segment the main image structures (water, oil slicks and ships) into distinct classes, thus showing the importance of accounting for the incidence angle.

Model

The log-intensities are modeled as a mixture distribution, maintaining the same principles as previously developed segmentation algorithms for SAR data [1]. The mixture components (classes) are assumed to be Gaussian along constant incidence-angle azimuth lines, with mean values expressed as a linear function of the given incidence angle [2]: $a_k + b_k\theta$. Each class is therefore defined by a triplet of parameters: covariance Σ_k, slope b_k and intercept a_k. After including the class weights π_k, the model becomes:

$$p_{X,\Theta}(x,\theta) = \sum_{k=1}^{M} \pi_k \frac{1}{(2\pi)^{d/2}\Sigma^{1/2}} e^{-\frac{1}{2}(x-(a_k+b_k\theta))^T\Sigma^{-1}(x-(a_k+b_k\theta))}. \quad (1)$$

Once the posterior probabilities (membership weights) z_{ik} are computed, the class parameters are estimated using Expectation-Maximization equations, i.e.:

$$a_k = \frac{\sum_{i=1}^{n} z_{ik}x_i - b_k\sum_{i=1}^{n} z_{ik}\theta_i}{\sum_{i=1}^{n} z_{ik}}, \quad (2)$$

$$b_k = \frac{\sum_{i=1}^{n} z_{ik}\theta_i x_i - a_k\sum_{i=1}^{n} z_{ik}\theta_i}{\sum_{i=1}^{n} z_{ik}\theta_i^2}, \quad (3)$$

$$\Sigma_k = \frac{\sum_{i=1}^{n} z_{ik}(x_i-(a_k+b_k\theta_i))(x_i-(a_k+b_k\theta_i))^T}{\sum_{i=1}^{n} z_{ik}}. \quad (4)$$

Segmentation of UAVSAR data

The incidence-angle dependency of the measurements collected from the UAVSAR platform was analyzed for all 4 polarimetric channels, by manually selecting a homogenous open-water area. Prior to analysis and segmentation a **15x60 multilook** window was applied.

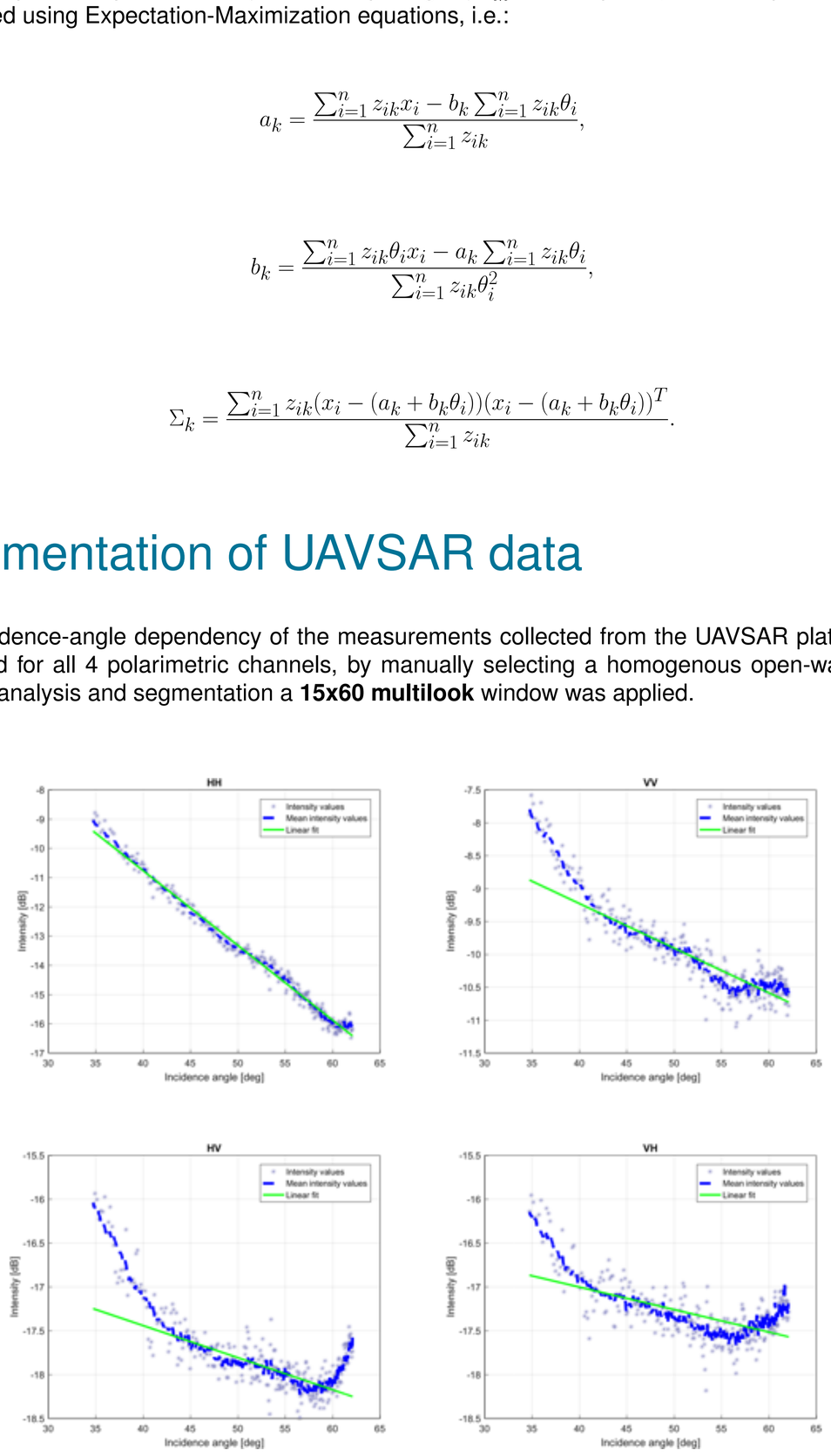

Figure 1: *Incidence-angle dependent decay rates of log-intesities measured with the UAVSAR instrument, for all polarimetric channels.*

The linear approximation of the decay rate is applicable throughout the entire 30 to 60 degree range only in the HH channel, suggesting the need for a different model for the other channels.

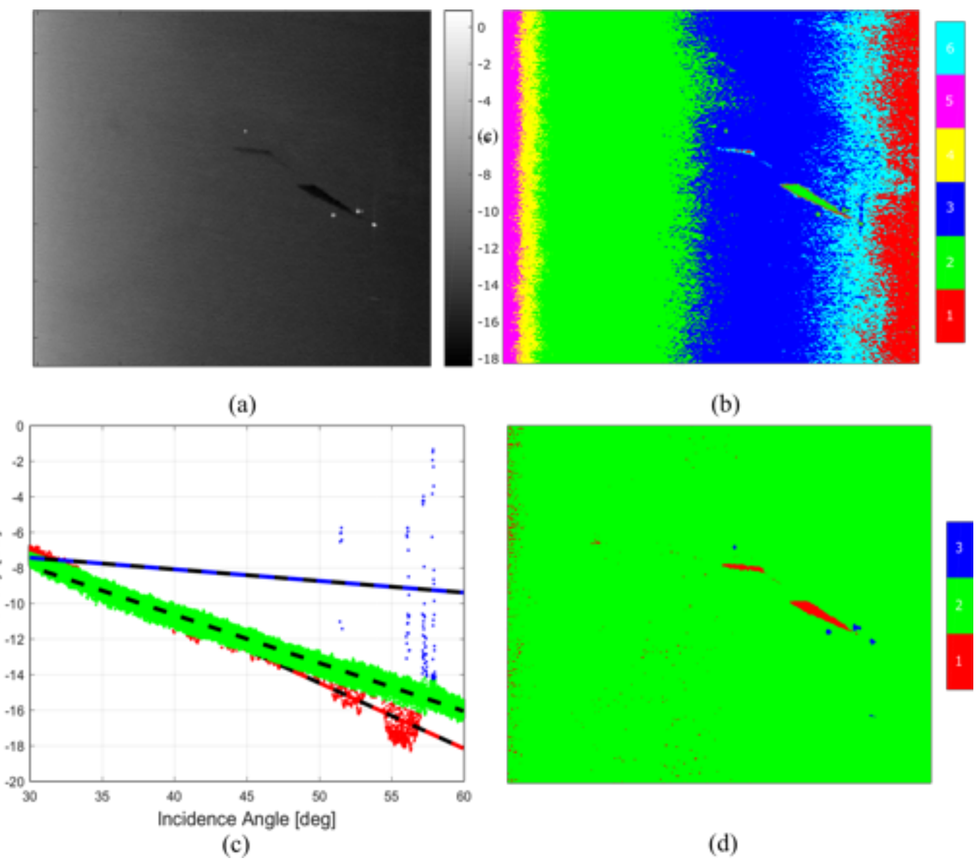

Figure 2: *Scene 1: Oil slicks and ships in the open sea. (a) HH intensities. (b) Segments obtained without considering the incidence angle. (c) Intensity decay rates per class. (d) Segments obtained considering the incidence angle.*

Scene 1 shows an oil spill detectable without considering the incidence-angle effect. However, the effect still causes banding, and the oil slicks appear in the same class as one of the bands. The new method eliminates banding and connects the open water regions in one class, while also identifying a separate class for the oil slicks and one for the previously undetected ships.

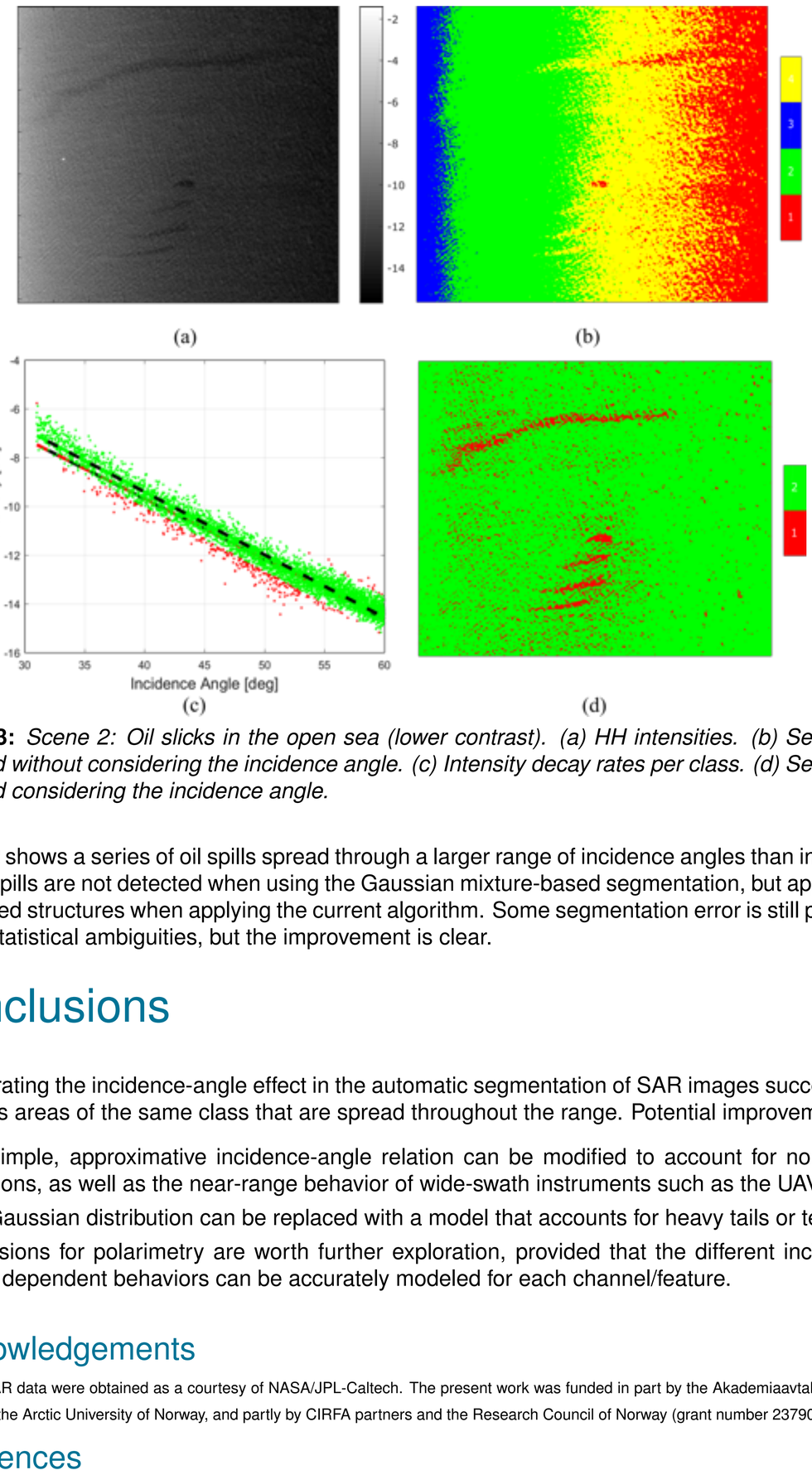

Figure 3: *Scene 2: Oil slicks in the open sea (lower contrast). (a) HH intensities. (b) Segments obtained without considering the incidence angle. (c) Intensity decay rates per class. (d) Segments obtained considering the incidence angle.*

Scene 2 shows a series of oil spills spread through a larger range of incidence angles than in Scene 1. The spills are not detected when using the Gaussian mixture-based segmentation, but appear as connected structures when applying the current algorithm. Some segmentation error is still present, due to statistical ambiguities, but the improvement is clear.

Conclusions

Incorporating the incidence-angle effect in the automatic segmentation of SAR images successfully connects areas of the same class that are spread throughout the range. Potential improvements:

- The simple, approximative incidence-angle relation can be modified to account for non-linear variations, as well as the near-range behavior of wide-swath instruments such as the UAVSAR.
- The Gaussian distribution can be replaced with a model that accounts for heavy tails or texture.
- Extensions for polarimetry are worth further exploration, provided that the different incidence-angle dependent behaviors can be accurately modeled for each channel/feature.

Acknowledgements

The UAVSAR data were obtained as a courtesy of NASA/JPL-Caltech. The present work was funded in part by the Akademiaavtale between Statoil and the Arctic University of Norway, and partly by CIRFA partners and the Research Council of Norway (grant number 237906).

References

1. A. P. Doulgeris, "A Simple and Extendable Segmentation Method for Multi-Polarisation SAR Scenes," in *The 6th International Workshop on Science and Applications of SAR Polarimetry and Polarimetric Interferometry (POLinSAR 2013)*, (Frascati, Italy), January 28 - February 1 2013.
2. W. Lang, P. Zhang, J. Wu, Y. Shen, X. Yang,"Incidence Angle Correction of SAR Sea Ice Data Based on Locally Linear Mapping," *IEEE Transactions on Geoscience and Remote Sensing*, vol. 54, no. 6, pp. 3188–3199, 2016.